JCSE The Journal of Corrosion Science and Engineering

21st Century Corrosion Science

Volume 6 Paper C121

# Microstructure and Corrosion Resistance of Laser Clad Ferrite-based Coatings with Rare Earth $La_2O_3$

G.M. Zhao, K.L. Wang

*Department of Mechanical Engineering, Tsinghua University, Beijing, 100084, P. R. China*

## Abstract

The Ferrite-based alloy powders with different contents of $La_2O_3$ were laser-clad onto steel substrate. The microstructural features and phase structure of these coatings were studied by scanning electron microscope (SEM) and X-ray diffraction (XRD), respectively. The results showed that the microstructure of the coatings with $La_2O_3$ was refined and purified and the main phase of the coatings was γ (Fe,Ni). Moreover, the electrochemical properties of the coatings were investigated by anodic polarization curves and electrochemical impedance spectroscopy (EIS). Anodic polarization results indicated that both polarization potential and polarization current density were reduced with the addition of $La_2O_3$. EIS results showed that, with the increasing of $La_2O_3$, the inductive arcs shrunk and capacitive arcs expanded. The inductive arc at low frequency was disappeared and fully changed to capacitive arc when the $La_2O_3$ addition reached 1.2wt%. The corrosion weight loss experimental results showed that the corrosion rate was lower and the corrosion attack was lighter in the coatings with $La_2O_3$ than that without $La_2O_3$, resulting in a substantial improvement of the corrosion resistance.

*Key words*: Laser Clad Coating; Rare Earth $La_2O_3$; Corrosion Resistance; Electrochemical impedance spectroscopy.

## 1. Introduction

Ferrite-based alloy was widely used in industry for its high performance-to-price ratio compared with other alloys. It has been well known that ferrite-based alloy has perfect properties of wear resistance, but its corrosion resistance is not very satisfied. How to improve its corrosion resistance is a key to expend the application of ferrite-based alloy.

In order to improve the corrosion resistance of ferrite-based alloy, adding some rare earth oxide to alloy powder through laser cladding has been widely studied [1-5]. However, there is still very little published on the research of corrosion resistance by testing the electrochemical properties, especially through EIS method. In this paper, the effect of $La_2O_3$ on polarization properties and impedance spectroscopy characters of ferrite-based alloy coatings were studied through anodic polarization curves and EIS spectra. The process of polarization was analyzed and the effect of RE on the electrochemical impedance was also discussed.

.

## 2. Experimental procedure

2.1 Experimental materials

The substrate material used was low alloy steel(AISI1115), which was cut to yield 100mm×20mm×10mm specimens. The chemical composition in wt.% was 0.12~0.20%C, 1.2~1.6% Mn, 0.2~0.6%Si and the rest Fe. Ferrite-based self-fluxing alloy powder of size 60+160 mesh was chosen as laser cladding material. The chemical composition of the powder in wt.% was 0.21%C, 1.18%B, 3.25%Si, 19.92%Cr, 12.6%Ni and the rest Fe. $La_2O_3$ was added into the ferrite-based alloy powder in different ratios in wt.% were 0%、0.4%、0.8%、1.2% and 2.0%, which were marked as 0#, 1#, 2#, 3# and 4# specimens, respectively. Alloy powder and $La_2O_3$ powder were mixed uniformly. After those procedures, the mixture was dried in a desiccator and preserved in a seal container.

2.2 Laser cladding parameters

Laser cladding was achieved by continuous wave $CO_2$ laser remelting flame sprayed coatings. The laser was operated at 1.5kw, and the laser beam was defocused to 3mm in diameter. The laser traverse speed was 5mm/s and the power density was $1.19\times10^4 w/cm^2$. Nitrogen gas was used to minimize oxidation. In order to get continuous coatings, the cladding was overlapped with ratio of 30%.

2.3 Instruments and corrosion test methods

Scanning electron microscope with energy-dispersive analysis of X-rays (EDAX) was used to observe the microstructure of coatings. A D/max-RB model X-ray diffractometer was used to determine the phase structure of the coatings. The experimental condition were CuKa radiation; tube voltage 40Kv; tube current 100mA.

Corrosion experiments were performed in three ways: anodic polarization、electrochemical impedance spectroscopy and weight loss.

By means of a potentiostat, the anodic polarization curves of laser clad coating specimens with different addition of $La_2O_3$ were measured in different solutions: 1mol/L $H_2SO_4$，1mol/L $HNO_3$, 1mol/L $H_3BO_3$ and 3% NaCl. A saturated calomel electrode was used as reference, and Pt was employed as the auxiliary electrode.

The EIS experiments were operated in 3% NaCl solution. The measurements were made using a lock-in amplifier coupled to a Potentiostat-Galvanostat system (Model M128), which was connected to a three-electrode electrochemical cell. A Pt foil was used as counter electrode and a saturated calomel electrode (SCE) was used as a reference electrode. The treated laser clad specimens were used as the working electrodes. The exposure area of laser clad coatings was $1cm^2$ and the test was processed in room temperature. EIS spectra were obtained at open-circuit potential of the specimens, with amplitude of 5mV. The frequency span was from 10KHz down to 0.01Hz. Data registration and analysis were performed on an interfaced computer. The spectra were then interpreted using the nonlinear fitting procedure by Zplot software.

The weight loss was tested in 2mol/L $H_2SO_4$ and 1mol/L HCl＋1mol/L $HNO_3$ solutions, respectively. The corrosion morphologies were observed by SEM.

## 3. Results and discussion

*3.1. Microstructure observation*

The microstructure of clad coatings with different $La_2O_3$ addition was observed by SEM and presented in Fig.1, Fig.2 and Fig.3. Fig.1 was the morphology near the interface between coating and substrate. Fig.2 and Fig.3 were the morphologies of middle zone and near-surface zone, respectively. It can be seen that the structure was far from uniform because of the different solidification speed. Fig.1 included three kinds of structures: one was planar band. It was the interface of solid and liquid at the beginning of the solidification. The other two kinds were cellular grains and dendrites. Fig.2 were a mixed structure of needle-like grains and dendrites. The most were needle-like grains and radiately distributed. In Fig.3, there are big dendrites with little needle-like grains and the latter distributed at the boundary of big dendrites.

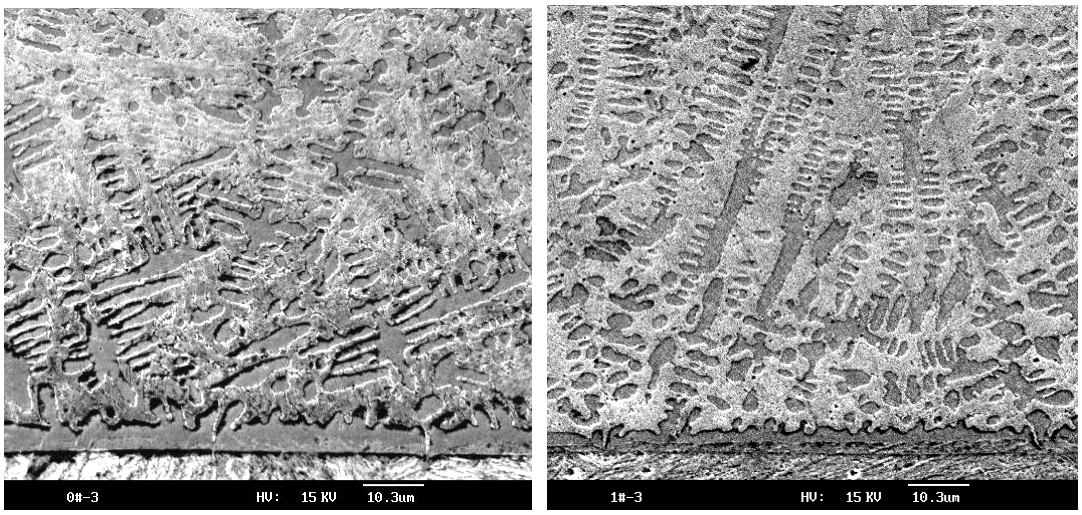


（a） (b)

Fig.1. SEM morphologies of microstructure of the laser clad coatings (near the interface): (a) without $La_2O_3$ and (b) with 0.4% $La_2O_3$.

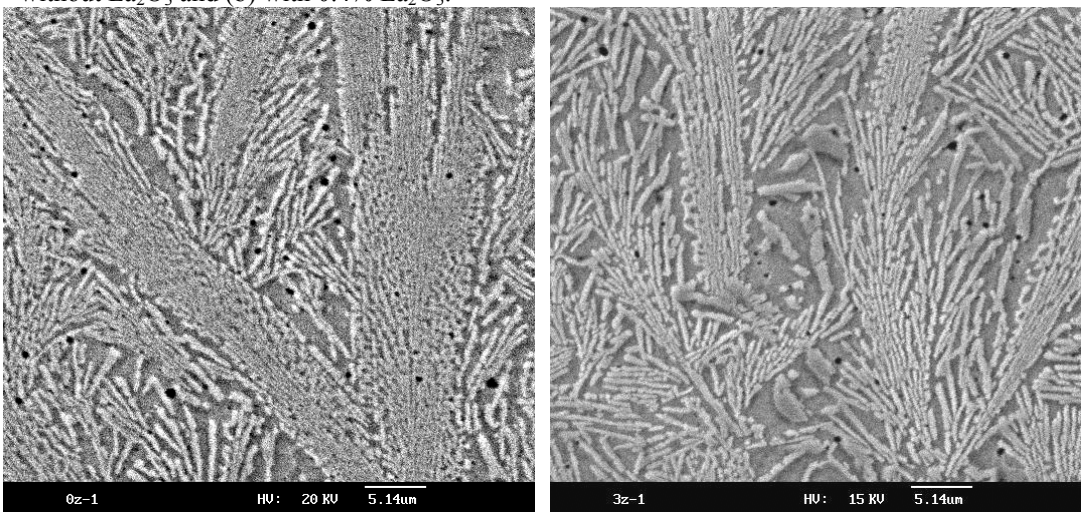


（a） (b)

Fig.2. SEM morphologies of microstructure of the laser clad coatings (from interface 100~120um): (a) without $La_2O_3$ and (b) with 1.2% $La_2O_3$.

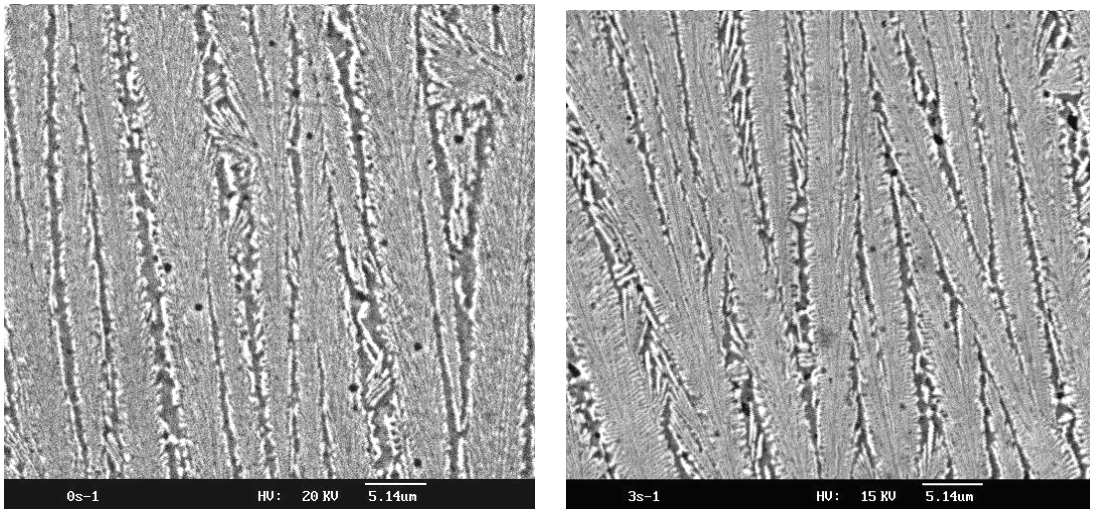


（a） (b)

Fig.3. SEM morphologies of microstructure of the laser clad coatings (near the surface): (a) without $La_2O_3$ and (b) with 1.2% $La_2O_3$.

It can be seen that all parts of structure were refined in some degree with $La_2O_3$ compared with those without $La_2O_3$. In Fig.1, with the addition of $La_2O_3$, the width of planar band was reduced from 5 μm to 3 μm, the secondary dendrite spacing was decreased from 10 μm to 5 μm and the transition zone between the planar band and cellular grains was expended. This indicated that the fluidity of the alloy liquid was increased [6], the over cooling induced by composition was decreased and the element segregation was reduced. In Fig.2, with the addition of RE, the direction of dendrites was weakened and the amount of the needle-like structure was increased. Moreover, when the addition of rare earth reaches 2.0(wt)%, the needle-like structures were interlaced, which decreased the distance between needle-like grains and restrained the growth of dendrites, resulting in the refinement of structure. In Fig.3, the distance between the big dendrites was decreased, making the boundaries of dendrites more compact. In this area, the growth of dendrites had the same direction in these zones because of the unilateral thermal transition.

3.2 Phase structure of laser clad coatings

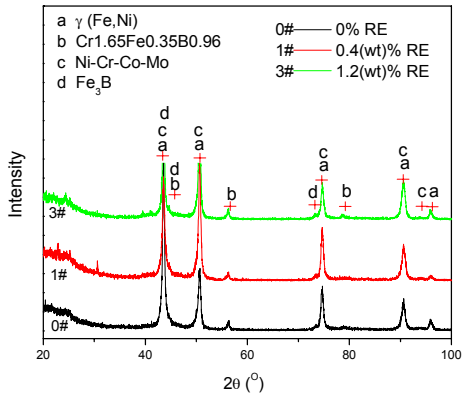


Fig.4. X-ray diffractograms of laser cladding with different addition of $La_2O_3$.

From XRD diagram (Fig.4), the main phase of the coatings was γ (Fe,Ni). There also included some others such as Cr1.65Fe0.35B0.96 and Ni-Cr-Co-Mo et al. With the addition of $La_2O_3$, the phase composition was not remarkably changed except the formation of $FeB_2$.

3.3 Electrochemical properties of coatings

3.3.1 Electrochemical impedance spectroscopy

Fig.5 was the result of EIS experiment. The a,c,e figures were the curves of nyquist and their fitted results. Zi was imaginary part of impedance and Zr was real part. The b, d, f figures were the curves of bode and their fitted results. Based on reference [7], the EIS spectra were the type of anode Farady impedance.

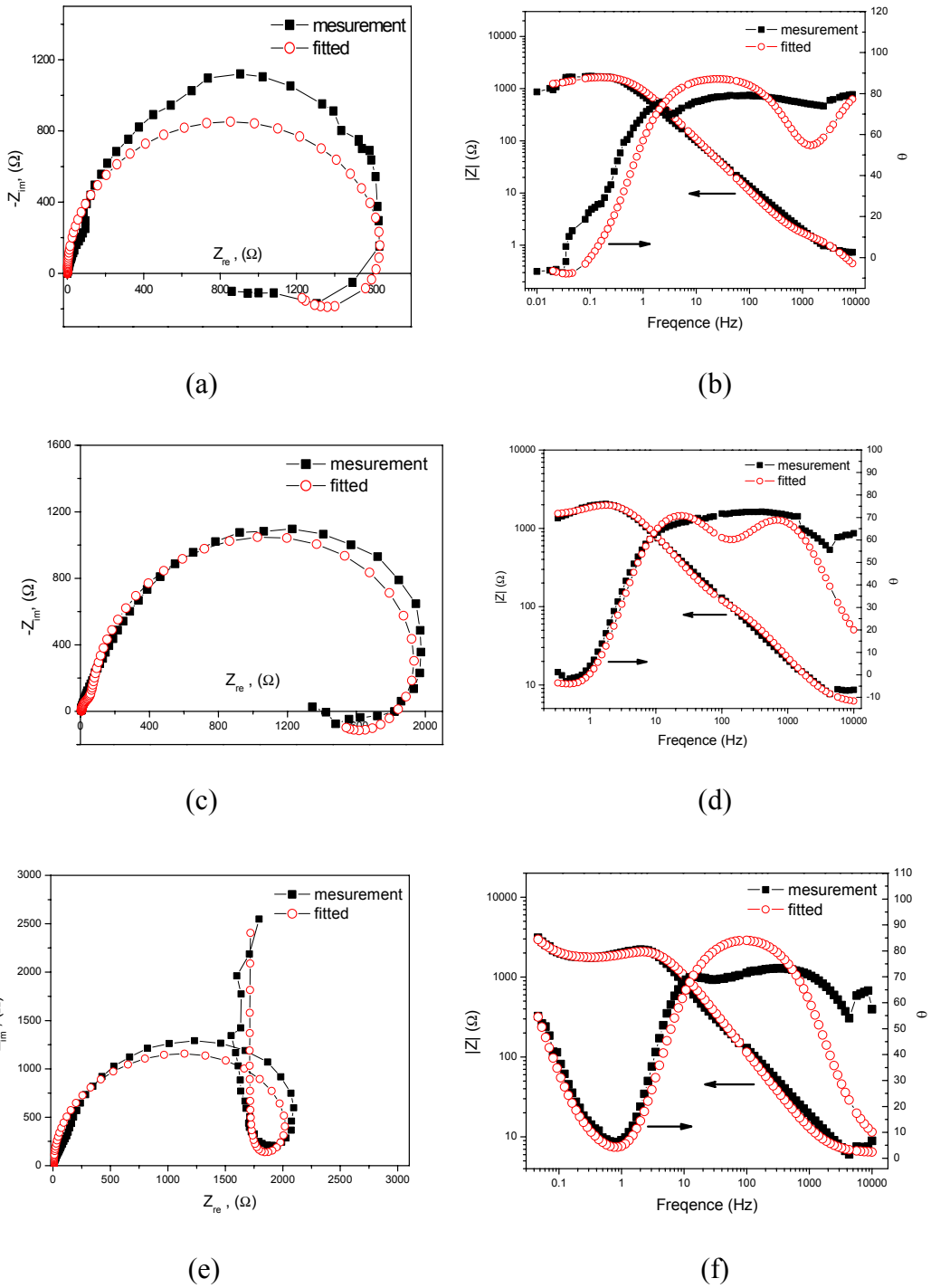


Fig.5. Plots of nyquist and bode of laser clad coatings: (a-b) without $La_2O_3$, (c-d) with 0.8% $La_2O_3$ and (e-f) with 1.2% $La_2O_3$.

Fig.5 showed that the three cases of impedance spectra had tow time loops. The EIS spectra of the

coating without $La_2O_3$ were mainly composed of an inductive arc at low frequency and a capacitive arc at high frequency. The capacitive arc at high frequency reflected the electrochemical reaction process on the surface of electrode [8]. In this case, the protective oxide film couldn't easily form on surface for the surface was in active status [9]. When $La_2O_3$ addition reached 0.8wt%, the impedance spectra were not clearly changed, but the capacitive arc in the low frequency was shrunk in some degree, indicating that the corrosion resistance was improved. When $La_2O_3$ addition reached 1.2%, there are still capacitive arc in high frequency, but the inductive arc in low frequency was changed to large capacitive arc. Based on reference [8], the capacitive arc at low frequency reflected the formation of passive film on surface during the process of metal's dissolution and this film can act as a protective barrier.

In NaCl solution, oxygen's deoxidation was the main reaction at cathode. The $OH^-$ ions were formed there and the PH value was increased. On the other hand, metal was dissolved and cations were formed at anode. The combination of anions and cations formed the passive film, covered on the surface of alloy and act as a protective layer. Fig.5 (e) showed the characters discussed above, indicating that the surface of electrode has produced thick passive film and the active pits on the surface decreased greatly.

Based on the characters of Fig.5, Fig. 6 was the equivalent circuit. After simulated and fitted by Zplot software, the values of different components were listed in Table 1.

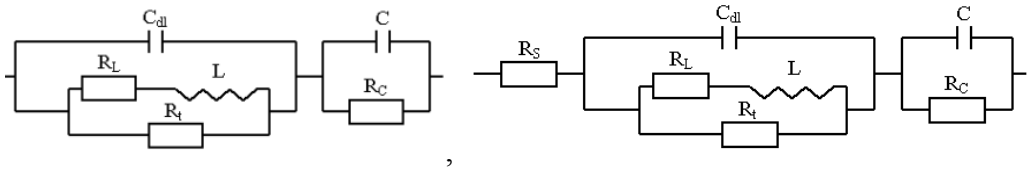


Fig.6. Equivalent circuit of coatings in NaCl solution: (a) with 0% $La_2O_3$, (b) with 0.8% $La_2O_3$ and 2.0% $La_2O_3$.

Table 1. The fitted results for EIS of coatings with different contents of $La_2O_3$

| $La_2O_3$ addition (wt.%) | Equivalent Circuit | $R_S$ (Ω) | $C_{dl}$ ($\times 10^{-5}$F) | $R_L$ ($\times 10^3$ Ω) | L ($\times 10^2$H) | $R_t$ ($\times 10^3$ Ω) | Rc (Ω) | C ($\times 10^{-5}$F) |
|---|---|---|---|---|---|---|---|---|
| 0 | Fig.6 (a) | / | 1. 458 | 3. 653 | 145. 3 | 1. 708 | 1.079 | 5. 332 |
| 0.4 | Fig.6 (b) | 5.829 | 1. 915 | 4. 128 | 8. 327 | 2. 130 | 59.76 | 1. 224 |
| 1.2 | Fig.6 (b) | 6.370 | 1. 410 | 6. 431 | 8. 431 | 2. 312 | 502100 | 142. 250 |

It can be seen that the difference between original results and fitted results was small. The departure was in the range of 10-20%. From reference [10-11], the results can be processed by semi-quantitative analysis, indicting that different coatings corresponded with different spectra. Generally speaking, the lower impedance at low frequency and the higher capacivity at high frequency, the severer corrosion of the coating. In this experiment, the capacity at high frequency was similar in value, but the impedance values in low frequency were $3.653\times10^3\Omega$, $4.128\times10^3\Omega$, $6.431\times10^3\Omega$, respectively. The values were in accession, indicating the descendant corrosion attack of these coatings.

The effect of $La_2O_3$ on electrochemical properties of laser clad coatings can be explain by the follow two aspects:

1. $La_2O_3$ can refine the structure of coatings and make the surface of the coatings possess an impact microstructure. Therefore, the number of micro-cells was decreased and the trend of electrochemical reaction was weakened.

2. For the active properties of RE, the formation free energy of oxide compound with RE was decreased. The coating can form a full passive film in low polarization potential. Thus, the corrosion rate was decreased, which can be seen by the change of Rt: the value of Rt was increased with the increase of RE.

3.3.2 Anodic polarization curves

The results of anodic polarization experiment were showed in Fig.7, where i and E represented

the polarization current density and polarization potential, respectively.

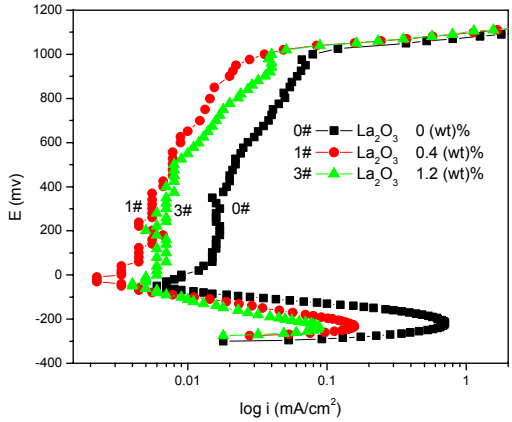


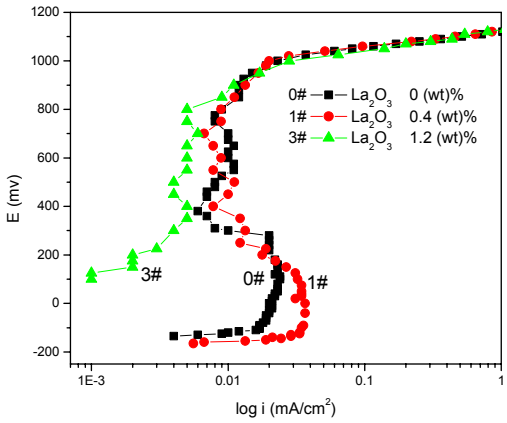


(a) (b)

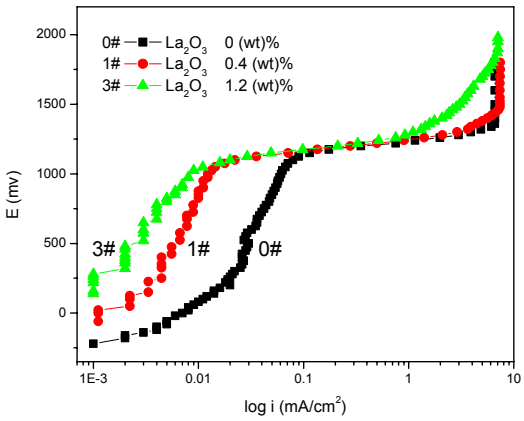

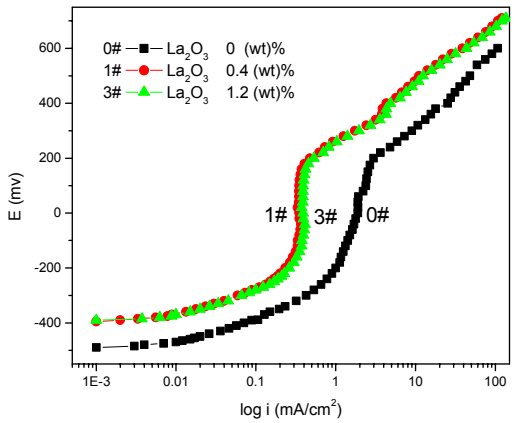


(c) (d)

Fig.7. Anodic polarization curves of laser clad coatings: (a) 1mol/L $H_2SO_4$, (b) 1mol/L $HNO_3$，(c) 1mol/L $H_3BO_3$ and (d) 5%NaCl.

The corrosion current density, which was represented by the polarization current density in curves, was proportioned to the corrosion rate [12]. Thus, the corrosion rate could be compared by the polarization current density at the same potential. Fig.7 shows that the polarization current density of coatings with $La_2O_3$ was lower than that without $La_2O_3$ in both salt and acidic solutions except the 1# sample in $HNO_3$ solution. This indicated that the coatings with $La_2O_3$ were polarized in lower current density and the rate of corrosive dissolution was decreased [13].

The corrosion reaction of ferrite-based alloy was hydrogen depolarization in acid environment. Fe was oxidized to $Fe^{2+}$ at anode, whereas $H^+$ was deoxidized to $H_2$ at cathode. RE can act as a barrier in permeation of $H_2$ [8], which inhibited the infiltration of hydrogen in ferrite and restrained the freedom of hydrogen. Thus, the activation coefficient of hydrogen was reduced and the reaction of cathode was slowed. On the other hand, the surface structure was unified with the addition of $La_2O_3$, the refinement of structure and the purification of the grain boundaries eliminate the defects and make corrosion reaction happening on these areas more impossible.

3.4 Weight loss experiment

Fig.8 was the curves of weight loss vs. $La_2O_3$ addition in different immersion time in 1mol/L $H_2SO_4$ and 1mol/L $HNO_3$ solutions, respectively. It showed that the corrosion rate was decreased after the addition of $La_2O_3$. This phenomenon became more obvious with the increase of immersion time. Fig.9 was the surface morphologies of coatings with and without $La_2O_3$ after immerged in 1 mol/L $H_2SO_4$ solution for 5 days and Fig.10 was in 1 mol/L $HNO_3$+1 mol/L HCl solution for the same time. They showed that the corrosion attack was not so severe in $H_2SO_4$ solution, where only the grain boundaries were eroded, due to the formation of passive film on the surface. Compared with the morphologies in Fig.9, there were many corrosion pits on the surface of the coating without $La_2O_3$, whereas that was hardly founded on the surface with RE. This indicated that the passive film could be more easily formed and the film was denser with RE, which decreased the defective pits on surface.

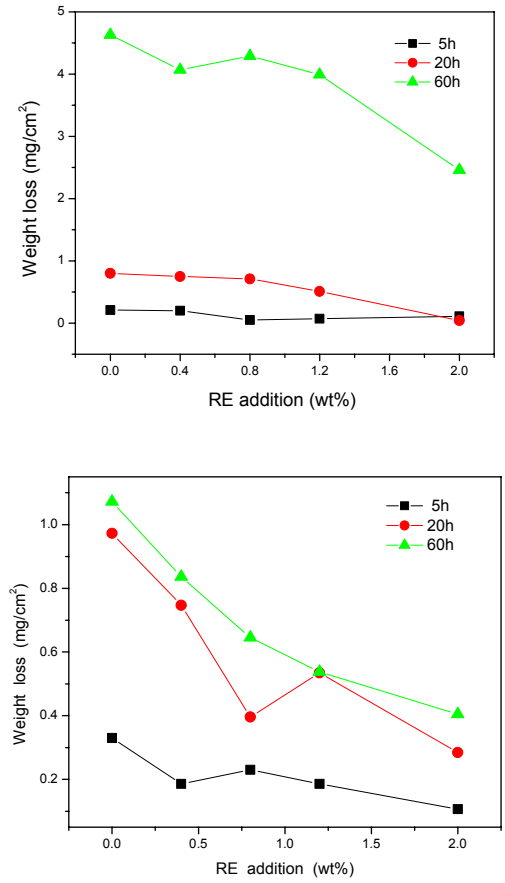


(a) (b)

Fig.8. Weight loss vs. $La_2O_3$ addition of laser clad coatings: (a) 1mol/L $H_2SO_4$ and (b) 1mol/L $HNO_3$.

Compared with Fig.9, the corrosion attack in Fig.10 was obviously deteriorated. In Fig.10 (a), there were many cracked, dispersive oxide scales and many deep grooves between the scales on the surface of coating without RE. The scales were warped, indicating the weak adherence and easily scaling off. Fig.10 (b) was the morphologies of coatings with 1.2% $La_2O_3$ after immerged in the same solutions for the same time. There wasn't any large area groove and large-scale spallation on the surface except some small pits.

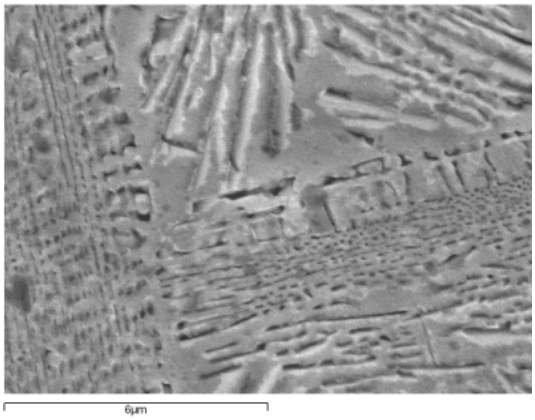

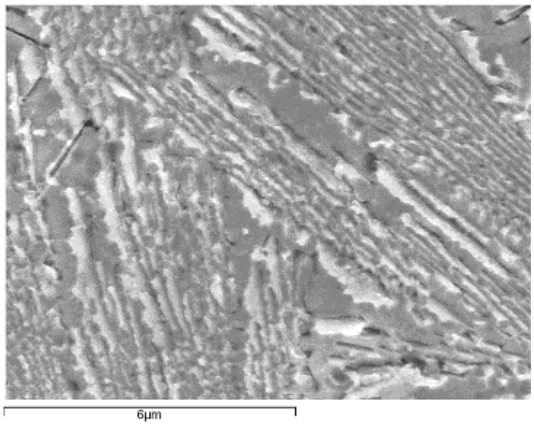


(a) (b)

Fig.9. Corrosion morphologies of laser clad coatings with in 1mol/L $H_2SO_4$ solution: (a) without $La_2O_3$ and (b) with 1.2% $La_2O_3$.

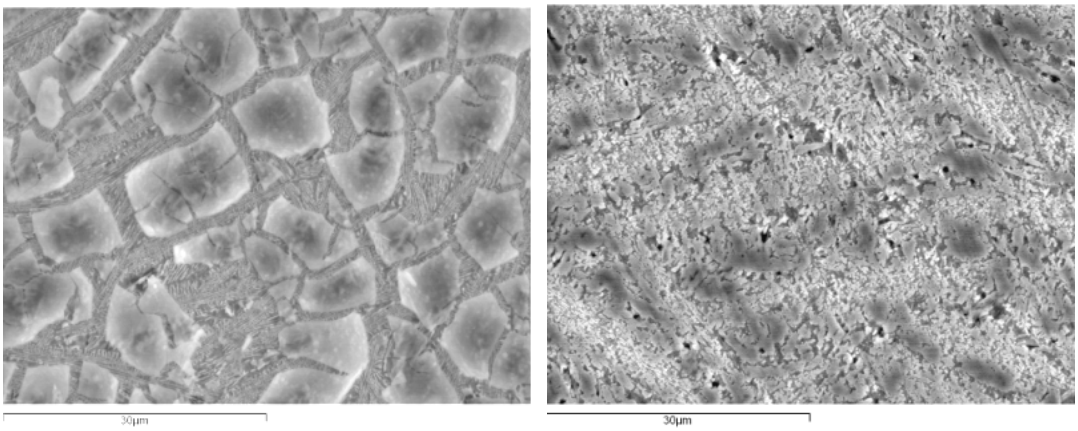


(a) (b)

Fig.10. Corrosion morphologies of laser clad coatings in 1mol/L HCL+1 mol/L$HNO_3$ solution: (a) without $La_2O_3$ and (b) with 1.2% $La_2O_3$.

Fig.11 was the corrosion morphologies of transition zone and near transition zone of overlapping. It can be seen that the former had better corrosion resistance than other parts of surface. In the transition zone, blurry grain boundaries and many erosion grooves was founded in the specimen without $La_2O_3$ (Fig11 (c, e)), indicating that there happened some spallation. But in Fig11 (d, f), the surface was unified and the corrosion only happened at inter-dendrite. Near the transition zone, many warped scales were observed on the surface of the specimen without $La_2O_3$ (Fig.11 (a, c)), indicating severe corrosion happened there with severe spallation. In contrast, the specimen with $La_2O_3$ had a smooth, unified and compact corrosion morphologies on the surface, where the needle-like structures were connected each other to form a network, greatly decreased the spallation of corrosion resultant.

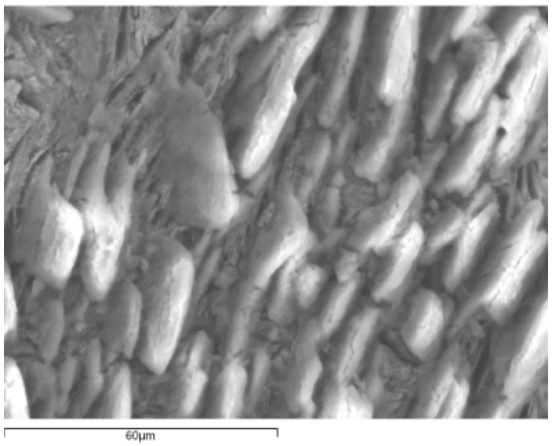


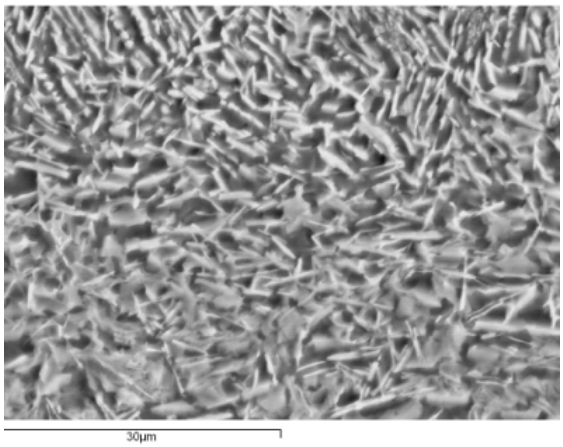


(a) (b)

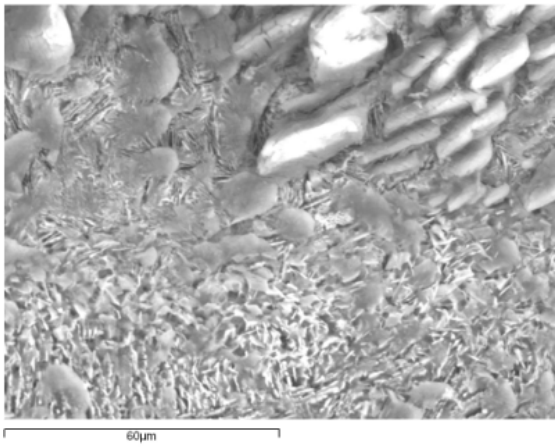

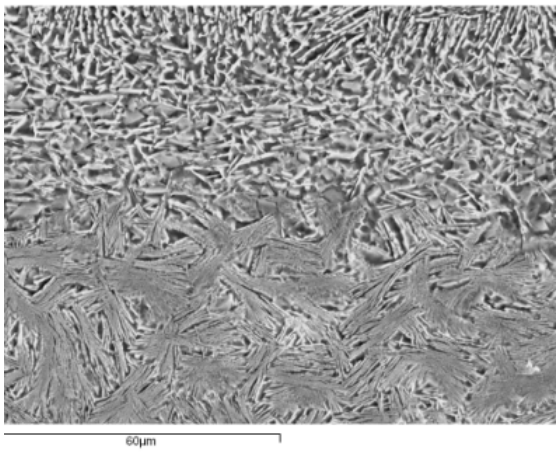


(c) (d)

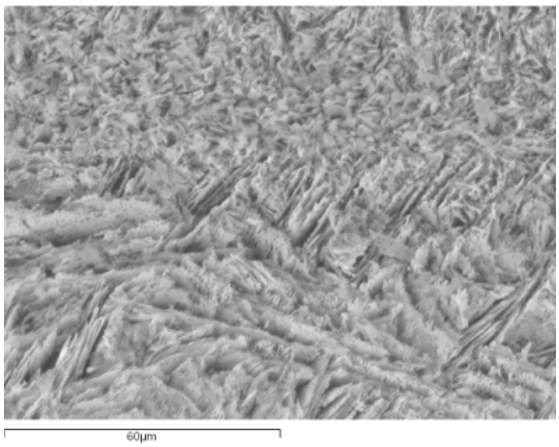


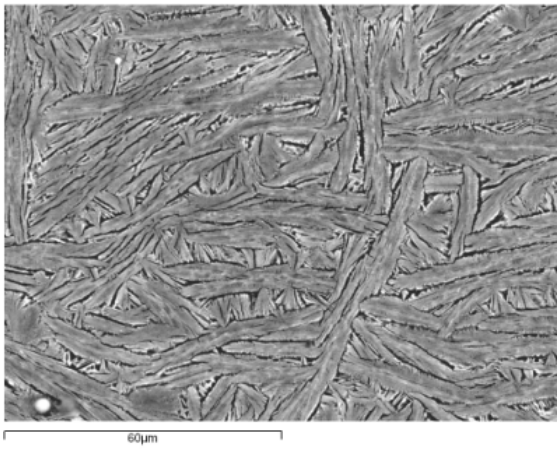


(e) (f)

Fig.11. Corrosion morphologies of transition zone and near transition zone of overlapping: (a,c,e) without $La_2O_3$ and (b,d,f) with 0.4% $La_2O_3$. ((a),(b) near the transition of overlapping (c),(d) the interface of transition and near transition (e)(f) the transition of overlapping)

The refinement and purification effect of the RE makes the microstructure more compact and unified, which was the main benefit in corrosion resistance. In addition, as active elements, RE can easily exist on the surface and reduce the oxidation potential of Cr, Ni elements. Thus, Cr, Ni ions can easily combine with acid radical to form steady compound. For the passivation character of those compounds, they can act as a barrier to hamper the processing of deep erosion, resulting in the low corrosion rate.

## 4. Conclusion

Addition of rare earth oxide $La_2O_3$ to laser clad ferrous-based alloy coatings results in the following:

1. Addition of $La_2O_3$ can effectively refine the microstructure, and make it become more unified and compact.
2. There are two or three loops in the EIS curves of all coatings. The curve without $La_2O_3$ mainly consisted inductive arc at low frequency and capacitive arc at high frequency. With the increasing addition of $La_2O_3$, inductive arc was shrunken and changed to a capacitive arc. Moreover, the impedance was increased with the addition of $La_2O_3$ and the electrochemical properties were improved at the same time.
3. With the addition of $La_2O_3$, the cathode reaction was slowed and the polarization current density was decreased in both salt and acidic solutions.
4. With the addition of $La_2O_3$, the active properties of surface make the protective film easily formed and hence facilitate the surface passivation. Thus, the corrosion rate was decreased.

## References


[1] Fan P., Yi W. and Zheng C.Q., *J. of the Chinese Rare Earth Soc.*, 4 (1999) 46
[2] Wang K.L, Zhang Q.B. and Sun M.L., *Corrosion Soc.*, 43 (2001) 255
[3] Wang K.L., Zhang Q.B. and Wei X.G., *Tsinghua University Transaction*, 39 (1999) 5
[4] Xu Y., Ji H. and Wei Y.D., *Chinese Rare Earth*, 22 (2001) 51
[5] Li A.M and Xu B.F., *Chinese Surf. Tech.*, 31(2002) 40
[6] Zhang L.Q. and Chen G.N., *Metal Heat Treatment*, 27 (2002) 10
[7] Cao C.N. and Zhan J.Q., *An Introduction to Electrochemical Impedance Spectroscopy*, China Science Press, Beijing, 2002, p.145
[8] Wang C., Zhang Q.S. and Jiang F., *Acta Metall. Sinica*., 38 (2002) 765
[9] Chen C.F., Lu M.X. and Zhao G.X., *Acta Metall. Sinica.*, 38(2002) 770
[10] Hu Y.L., Li D. and Guo B.L., *J. of the Chinese Society for Corrosion and Protection*, 22 (2002) 8
[11] C.X.Wang and M.Wang. *Materials Letters*, 54 (2002) 30
[12] N.Eliaz, D.B.Mitton and N.J.cantini, *Mat.Tech. & Adv.Perf.Mat.*, 16 (2000) 90
[13] Xu Y., Ji H. and Chen X., *J of the Chinese Rare Earth Soc*., 19 (2001) 346